

Human Whole-Blood Relaxometry at 1.5T: Assessment of Diffusion and Exchange Models

Bojana Stefanovic* and G. Bruce Pike

Human whole-blood relaxometry experiments were performed to allow the prediction of blood signal changes with blood oxygen saturation (Y) and refocusing interval (τ_{180}). Such predictions are particularly relevant for spin-echo (SE) blood oxygenation level-dependent (BOLD) experiments and a recently proposed noninvasive fMRI method for measuring cerebral blood volume (CBV). Ensemble fitting of the entire set of T_2 estimates, obtained over an extensive range of Y and τ_{180} values, was performed with the use of both a fast chemical exchange model and a model of diffusion in weak magnetic field inhomogeneities. The diffusion modeling resulted in a large reduction in the residual sum-of-squares compared to the fast exchange modeling. The longitudinal relaxation rate decreased linearly with Y , and increased with hematocrit. The results support the application of the recently reported diffusion model to describe deoxyhemoglobin (dHb)-induced blood transverse relaxation rate enhancement at 1.5 T. Magn Reson Med 52: 716–723, 2004. © 2004 Wiley-Liss, Inc.

Key words: blood; relaxation; diffusion; exchange; refocusing interval

Due to the paramagnetic nature of deoxyhemoglobin (dHb), partial deoxygenation of blood leads to the establishment of microscopic magnetic field gradients and, consequently, an enhanced rate of spin dephasing. This effect is widely exploited in blood oxygenation level-dependent (BOLD) fMRI. Both extra- and intravascular compartments contribute to the total BOLD response, with the relatively long exchange time of water across the capillary wall (on the order of 0.5 s (1)) rendering the two compartments separate on the time scale of an MRI experiment. Despite a very small cerebral blood volume (CBV) fraction, the increase in the T_2 of blood oxygenation is so much greater than that of tissue that almost all of the spin-echo (SE) BOLD response at 1.5 T originates in the vasculature (2). This strong dependency of blood T_2 on the degree of oxygen saturation (Y) has been used for venous blood oximetry (3) and oxygen extraction measurements (4). The associated sensitivity of blood T_2 on the refocusing interval (5) was recently exploited to isolate the blood signal and noninvasively measure CBV changes (6). The accurate quantification of the physiological parameters of interest

via such techniques is contingent on the robust quantitative prediction of spin-spin relaxation in blood over the physiological range of Y and the refocusing intervals employed in a given acquisition. In this study, we set out to characterize the effect of blood oxygenation and the refocusing interval on T_2 of whole human blood, in the context of normal brain physiology.

Although numerous studies have been performed on red blood cell suspensions, whole bovine blood, and whole human blood to investigate the dependence of blood T_2 on various physiological parameters, a complete understanding of the underlying mechanism is still lacking. Invariably, these studies (3–10) reported a pronounced shortening of T_2 with deoxygenation and/or elongation of the refocusing interval. Qualitatively, this phenomenon clearly results from sequestration of paramagnetic dHb in red blood cells of partly deoxygenated blood (5). Quantitatively, however, much controversy remains. Various models have been proposed to explain the effect, including fast chemical exchange of water protons between the two compartments (3,4,7,8) and/or diffusion in the intra- and/or extracellular magnetic gradients (5,9,10). In view of the complexity of diffusion modeling (11), a number of researchers have used the exchange model as a convenient analytical approximation (10). Recently, Jensen and Chandra (12) described a detailed theoretical model of transverse relaxation rate enhancement in the presence of weak microscopic field inhomogeneities, and applied it to published Carr-Purcell-Meiboom-Gill (CPMG) data for isotonic and hypotonic red blood cell suspensions, using both canine and human blood. In turn, Brooks et al. (13) showed an equivalence between the chemical exchange model and the diffusion model in the short- and long-echo limits. Nevertheless, a considerable variability in the parameter estimates has been observed in practice across different studies employing either exchange or diffusion models (4,11).

In addition to spin-spin relaxation, the effect of deoxygenation on the spin-lattice relaxation time is also of interest, since the typical repetition time (TR) in an fMRI experiment (which is chosen to maximize temporal resolution) makes the resulting BOLD signal sensitive to T_1 variations. Moreover, a dependency of T_1 on Y (and hence the extent of T_1 variation across the vasculature) would affect perfusion quantification via arterial spin labeling (ASL) (14) techniques, dependent on blood signal isolation, as well as the aforementioned technique for CBV quantification (6). In contrast to a number of earlier studies (5,15,16), a recent report (14) documented a dependence of T_1 in blood on hematocrit as well as oxygen saturation.

McConnell Brain Imaging Centre, Montreal Neurological Institute, McGill University, Montreal, Canada.

Grant sponsors: Natural Sciences and Engineering Research Council of Canada; Canadian Institutes of Health Research.

*Correspondence to: Bojana Stefanovic, McConnell Brain Imaging Centre, Montreal Neurological Institute, 3801 University St., WB325, Montreal, Quebec H3A 2B4 Canada. E-mail: bojana@bic.mni.mcgill.ca

Received 3 February 2004; revised 7 May 2004; accepted 10 May 2004.

DOI 10.1002/mrm.20218

Published online in Wiley InterScience (www.interscience.wiley.com).

© 2004 Wiley-Liss, Inc.

The dHb-induced changes in T_1 , which are of much smaller relative magnitude than those of the transverse relaxation time, have been postulated to result from direct dipolar interactions of water protons with paramagnetic dHb (14).

To investigate relaxation mechanisms in whole human blood, particularly as they pertain to the brain activation physiology, we tested the current models of spin-spin relaxation in blood, and made in vitro estimates of each model's parameters while spanning the fMRI-relevant range of blood oxygenation levels and an extensive set of refocusing intervals. To complete the blood signal characterization, the dependence of T_{1blood} on Y and hematocrit was examined. Beyond obtaining insight into blood relaxation behavior, we strove to arrive at a robust parameterization of the best-performing model to enable precise quantification of intravascular SE signal changes following brain activation, and facilitate accurate measurements of the physiological parameters of interest in acquisition strategies that rely on the dHb-induced blood T_2 shortening phenomenon.

THEORY

The confinement of paramagnetic dHb to red blood cells gives rise to two vascular compartments (the intra-erythrocytic and the plasmatic) with distinct magnetic properties. The exact mechanism of the deoxygenation-induced shortening of the T_2 of blood has been variably ascribed to the transmembrane exchange of water spins between the two environments (8,17,18) and/or diffusion in the local intracellular (19), extracellular (20), or intra-/extracellular magnetic field gradients (5,9).

In the exchange model, the spins experience effectively instantaneous jumps between the two compartments (8). Following Luz and Meiboom's model of fast chemical exchange between two sites at different frequencies (21), the dependency of blood T_2 (T_{2b}) on the refocusing interval (τ_{180}) is given by

$$\frac{1}{T_{2b}} = \frac{1}{T_{20}} + \gamma^2 K_0 \tau_{ex} \left(1 - \frac{2\tau_{ex}}{\tau_{180}} \tanh \frac{\tau_{180}}{2\tau_{ex}} \right), \quad [1]$$

where T_{20} is the intrinsic T_2 of blood (here indicating the limiting T_2 of blood as the refocusing interval tends to zero); γ is the gyromagnetic ratio ($2.675 \times 10^8 \text{ rad/s/T}$); K_0 is the variance of microscopic spatial field inhomogeneities (12); and τ_{ex} is the average exchange time of a spin between the two compartments.

Alternatively, Jensen and Chandra (12) recently described the effect of weak microscopic field inhomogeneities on spin-spin relaxation in the presence of diffusion of significant magnitude relative to the length scale of the field inhomogeneities. The dependence of blood T_2 on the refocusing interval was described as (12):

$$\frac{1}{T_{2b}} = \frac{1}{T_{20}} + G_0 \frac{\gamma^2 r_c^2}{2D} F\left(\frac{2D\tau_{180}}{r_c^2}\right), \quad [2]$$

where G_0 is the mean squared magnitude of the field inhomogeneities; r_c is the characteristic length scale for

the spatial variations of the field inhomogeneities; and D is the diffusion coefficient. The function F is given by (12):

$$F(x) = \frac{1}{\sqrt{\pi}} \int_0^{\infty} \frac{e^{-y}}{\sqrt{y}} \left(1 - \frac{1}{xy} \tanh(xy) \right) dy. \quad [3]$$

MATERIALS AND METHODS

Blood Collection and Handling

Whole-blood specimens were obtained by venipuncture from four healthy adults on two separate occasions. The blood was drawn from the superficial veins of the non-dominant forearm into dry heparanized syringes (15 mm diameter, 3 mL draw; Becton Dickinson Vacutainer Systems, Franklin Lakes, NJ), with special care taken to avoid any air bubble formation in the vacutainer. The oxygen saturation was modified in vivo via exercise. Specifically, forearm occlusion was achieved by inflation (to ~50% above the subject's systolic pressure) of a blood-pressure cuff, positioned ~4 cm superior to the olecranon process. The first sample was drawn with the arm at rest. The subject was then instructed to lift a 5-lb hand weight repeatedly by alternating elbow flexion and extension (with the nondominant arm) for about 4 min. Another two blood samples were drawn in the course of the exercise. Finally, the forearm cuff was released and the last blood sample was drawn during the ensuing hyperoxymic stage. Informed consent was obtained prior to each session in accordance with institutional guidelines.

Immediately following the phlebotomy, the filled vacutainers were placed in a custom-built gear made of LEGO (Lego Group, Billund, Denmark). They were secured in a wooden frame, which was custom-built to fit into the transmit/receive CP extremity coil (Siemens, Erlangen, Germany), with the long axes of the vacutainers parallel to the applied static magnetic field. A long wooden rod connected the frame to a veristaltic pump (Manostat, New York), which allowed the vacutainers to be rotated about their long axes at ~20 rpm. The pump was connected to a custom-built switch, which received triggers from the scanner and provided the pump with power (hence enabling the gear rotation) only during the delay period at the end of each repetition (with the pump switched off 1 s prior to the readout). The chosen rotation frequency prevented the settling of erythrocytes, which is known to significantly affect the lineshape within 2–3 min (16,22,23), while minimizing the inertial motion of blood during readout. The rotation rate employed corresponds to an average linear velocity of <1 cm/s, and is hence representative of blood flow in the microvasculature (1).

Within 5 min after the MR relaxometry measurements were completed, the blood samples were analyzed with the use of a Bayer 800 series blood analyzer and co-oximeter system (Bayer AG, Leverkusen, Germany). Measurements of blood gases and oxygen status were corrected for the scanner room temperature (22°C). We performed co-oximetry on each sample to establish the content of hemoglobin and its derivatives, and estimate the hematocrit (Hct).

Blood Relaxometry

Two single-slice sequences were used for in vitro blood T_2 relaxometry: a T_2 -prepared segmented EPI sequence (24) ($2.3 \times 2.3 \times 5 \text{ mm}^3$) on the first set of blood samples, and a 32-echo CPMG sequence ($2 \times 2 \times 5 \text{ mm}^3$) on the second set of blood samples. The former sequence contained a nonselective T_2 -weighted preparation with a nonselective 90° excitation followed by a train of hard refocusing pulses with subsequent nonselective tip-up, slice-selective excitation, and segmented EPI readout. This scheme is particularly suited to the application at hand because it allows very short refocusing intervals to be probed, which is a critical issue considering the time scale of the exchange/diffusion processes being investigated. The refocusing intervals employed were 2, 2.5, 3, 3.74, 4, 4.5, 5, 7, 10, 12, 14, 17, 20, 30, and 40 ms. This sampling was motivated by a number of considerations: the expected high rate of change of T_2 blood with respect to the refocusing interval for $\tau_{180} < 10 \text{ ms}$, the comparison between the T_2 blood estimates from the T_2 -prepared EPI data with those of the CPMG acquisition, and the refocusing intervals employed in our CBV technique (6). The order of acquisitions with different refocusing intervals was randomized. To investigate the reproducibility of the blood T_2 estimates over the scanning window, we probed at least two randomly-selected refocusing intervals twice in the course of a scanning session. To minimize the confounding effects of imperfect slice profiles and sensitivity to B_1 inhomogeneities, we used nonselective composite 90°_x - 180°_y - 90°_x pulses for refocusing, with their phases following the MLEV pattern (25). Finally, a large spoiling gradient was applied following the slice-selective tip-up to dephase any remaining transverse magnetization. For each refocusing interval, six different T_2 preparation durations were run, providing six effective echo times (TEs), equally spaced over the sampling window, which extended from 20 to 120 ms for the shortest, and from 80 to 480 ms for the longest refocusing interval acquisitions, respectively. The acquisition parameters included a $150 \times 112.5 \text{ mm}$ FOV, with a 64×48 matrix, EPI factor of 3 (i.e., three k -space lines per readout), readout bandwidth of 616 Hz/pixel, and a 3-s TR.

We employed a 32-echo CPMG acquisition, the de facto standard for T_2 relaxometry (26), to test the robustness of the T_2 -prepared segmented EPI sequence in quantifying the T_2 of blood in vitro. The interecho intervals in the various CPMG sequence versions were 7.5, 8, 8.5, 9, 9.5, 10, 11, 12.5, 15, 17.5, 20, 25, 30, 35, and 40 ms. The sequence parameters were optimized to provide robust T_2 measurements with the shortest achievable interecho intervals. The CPMG variants were played out in randomized order. As before, nonselective composite 90°_x - 180°_y - 90°_x pulses were used for refocusing. To suppress stimulated echoes, flow effects, and signal contributions outside of the slice of interest, the refocusing pulses were flanked by spoiling gradients, alternating in sign and decreasing in magnitude (26). The total diffusion weighting due to these gradients was small, with $b < 1 \text{ s/mm}^2$ in the last echo. Identical crusher gradient amplitudes and timing with respect to the refocusing pulses in all versions of the CPMG sequence ensured identical b -values. A $256 \times 128 \text{ mm}$ FOV, with a 128×64 matrix, readout bandwidth of

315 Hz/pixel, and a 4-s TR were used in each CPMG acquisition.

The spin-lattice time constant of blood was quantified by means of a single-slice Look-Locker sequence (27) with a segmented EPI readout ($2.3 \times 2.3 \times 5 \text{ mm}$). A composite 90°_x - 180°_y - 90°_x pulse was used for nonselective inversion, with inversion time (TI) set to 15 ms. Each of the four 20° excitation pulses, applied every 495 ms, was followed by a readout with a TE of 10 ms. The readout bandwidth was set to 140 Hz/pixel, with a 150-mm readout FOV, 75% phase FOV, and 4-s TR. The total scan time per set of four blood samples was approximately 80 min. In each case, the imaging slice was 5 mm thick, perpendicular to the long axes of the vacutainers, and positioned at the center of the 20-mm-long, blood-filled compartment. Localized shimming was done on the imaging slice at the beginning of the experimental protocol. All of the studies were performed on a Siemens 1.5 T Magnetom Sonata system (Siemens, Erlangen, Germany).

Data Analysis

Nonlinear least-squares minimization was used to fit the multiecho data from both T_2 -prepared segmented EPI and CPMG acquisitions in the region of interest (ROI) at the center of each vacutainer (and hence avoiding any partial volume effect) to a monoexponential decay model. Subsequently, we calculated the repeatability quotient (28) within each method to assess the repeatability of the measures across time, and thereby test the effects of the erythrocytic metabolism over the course of the experiment on the T_2 estimates. The limits of agreement (28) between the two methods were computed to test the validity of using the T_2 -prepared segmented EPI acquisition for T_2 relaxometry. Both exchange and diffusion models were then fitted to the T_2 estimates derived from the T_2 -prepared EPI data. In each case, the nonlinear model fitting was performed with the use of a trust region method. For both model structures, two model orders were investigated: a constrained model, in which T_{20} was fixed across oxygen saturation levels; and an unconstrained one, in which the T_{20} was allowed to vary with Y . In all cases, a single common τ_{ex} for exchange or $r_c^2/2D$ for diffusion was imposed on all T_2 vs. τ_{180} curves, while K_0 (in exchange) or G_0 (in diffusion) varied with Y . An F-test was employed to select the optimal model order within each model structure. The dependence of the variance of microscopic spatial field inhomogeneities on the blood oxygen saturation level was also investigated. Nonlinear least-squares minimization was used to fit the monoexponential recovery model to the Look-Locker data. The dependence of the resulting T_1 estimates on Y was explored via nonlinear least-squares minimization, and two-way analysis of variance (ANOVA) was employed to assess the effect of hematocrit on the T_1 estimates.

RESULTS

T_2 Relaxometry

The mean difference across time for the repeated T_2 estimates ($N = 20$) using the T_2 -prepared multishot EPI acquisition was $0.1 \pm 1.7 \text{ ms}$ (mean \pm standard error). The

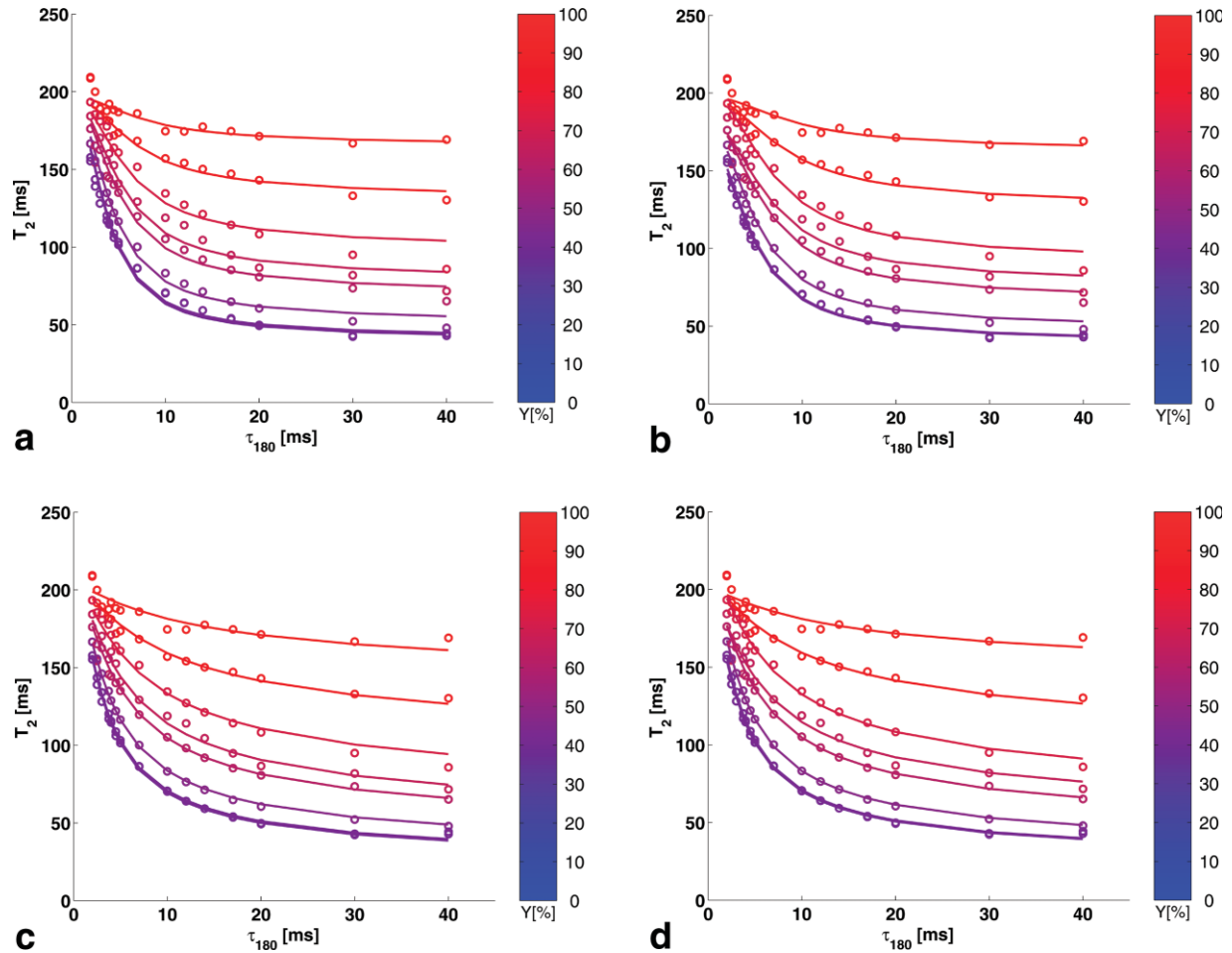


FIG. 1. T_2 blood estimates and the fits of the constrained (a) and unconstrained (b) exchange; and constrained (c) and unconstrained (d) diffusion models. The hematocrit of the blood samples employed was $51.2\% \pm 0.4\%$ (mean \pm standard error). Note the near coincidence of the bottom two curves, as expected given that the corresponding blood samples have very similar oxygenation ($Y = 42\%$ and 43% , respectively).

corresponding repeatability coefficient was 15 ms, so an absolute difference in the repeated T_2 estimates of <15 ms is expected in 95% of the cases given an approximately normal distribution of the differences (28). A higher repeatability was observed for the CPMG-based T_2 estimates ($N = 8$), as expected, with a mean difference across time of 0.0 ± 1.8 ms and a repeatability coefficient of 10 ms. The limits of agreement (i.e., 2 standard deviations (SDs) of the differences) for T_2 estimates ($N = 5$) from acquisitions with matched refocusing interval, blood oxygen saturation, and hematocrit using T_2 -prepared segmented EPI and 32-echo CPMG acquisitions were -7.8 ms to 2.7 ms (95% confidence interval of -13 ms to -2.1 ms for the lower bound, and -2.9 ms to 8.4 ms for the upper bound). The mean difference between the T_2 estimates of the two measurement techniques was -2.5 ms, with zero included in the 95% confidence intervals on this bias.

The set of T_2 estimates ($N = 120$), obtained from mono-exponential modeling of T_2 -prepared EPI data from blood samples with matched hematocrit ($51.2\% \pm 0.4\%$, mean \pm standard error), was fitted with the use of Eqs. [1] and [2]. Allowing for variation in the intrinsic T_2 of blood with the oxygenation level produced a better fit (at 0.01 level of significance) in the exchange, but not in the diffusion

modeling, as established by the F-test of the reduction in the sum of squared residuals (SSR), in going from constrained to unconstrained models within each model structure (P -values = 4.7×10^{-8} and 1.3×10^{-2} for the

Table 1
Exchange and Diffusion Model Parameter Estimates*

Y (%)	$T_{20,exchange}$ (ms)	K_0 ($10^{-14} T^2$)	G_0 ($10^{-14} T^2$)
93	198 ± 5	0.5 ± 0.1	0.8 ± 0.1
87	197 ± 5	1.4 ± 0.2	1.9 ± 0.2
72	200 ± 6	2.9 ± 0.4	3.7 ± 0.4
66	183 ± 7	3.7 ± 0.5	5.5 ± 0.6
62	184 ± 7	4.6 ± 0.6	6.6 ± 0.8
48	179 ± 9	7.3 ± 1.0	10.1 ± 1.2
43	169 ± 10	9.3 ± 1.3	13.2 ± 1.7
42	166 ± 10	9.4 ± 1.3	13.6 ± 1.8

*The exchange time (τ_{ex}) estimate was 3.0 ± 0.2 ms, with the intrinsic spin-spin relaxation time ($T_{20,exchange}$) and the curvature term (K_0) shown in columns 2 and 3. For the diffusion model, the characteristic length scale of spatial variations of field inhomogeneities (r_c) was 4.3 ± 0.2 μm (assuming a D of 2.0 $\mu\text{m}^2/\text{ms}$); and the intrinsic spin-spin relaxation time ($T_{20,diffusion}$), 203 ± 3 ms, with the curvature term (G_0) listed in column 4.

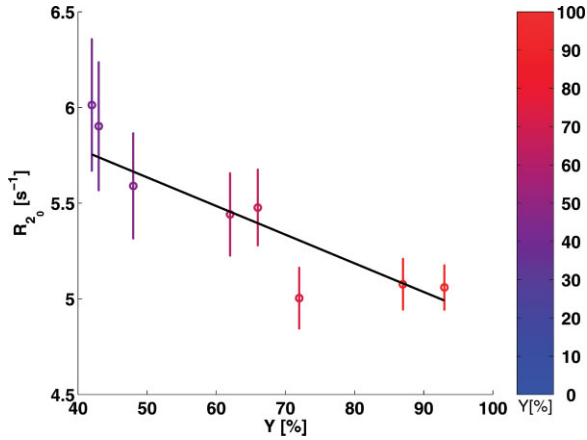


FIG. 2. The intrinsic blood spin-spin relaxation rate estimates from fast exchange modeling fitted against oxygen saturation. The intercept estimate was $1/(157 \pm 6) \text{ ms}^{-1}$, and the slope was dR_{20}/dY , $(-0.0150 \pm 0.0037) \times 10^{-3} \text{ ms}^{-1}/\%$. The SSR was $0.687 \times 10^{-3} \text{ ms}^2$, and the normalized mean squared error (NME) was 2.33×10^{-3} .

exchange and diffusion models, respectively). Furthermore, the comparison of the SSR for the selected model order within each model structure led to the selection of the diffusion model (since the constrained diffusion model produced a lower SSR than the unconstrained exchange model: $SSR_{diffusion} \sim 1.85 \text{ ms}^2$ and $SSR_{exchange} \sim 2.49 \text{ ms}^2$). The estimated blood T_2 values at different levels of oxygen saturation, as well as the fits of the unconstrained exchange and constrained diffusion models to these data, are shown in Fig. 1. Table 1 summarizes the results of this modeling.

Given the selection of the higher-order model within the fast exchange formulation, the intrinsic blood spin-spin relaxation time estimates from this modeling ($T_{20,exchange}$) were regressed against the blood oxygen saturation for comparison with literature values (cf., Fig. 2). A significant correlation was found: $r^2 \sim 0.83$ and $P \sim 4.8 \times 10^{-10}$. Following the expected dependencies (29), the estimates of the mean squared magnitude of the field inhomogene-

Table 2

The Fits of Mean Squared Magnitude of the Field Inhomogeneities Estimated from the Exchange (K_0 , First Row) and Diffusion (G_0 , Second Row) Models Against $(1-Y/100)^2$

Slope (10^{-13} T^2)	SSR (10^{-27} T^4)	NME (10^{-15})
3.1 ± 0.2	1.37	1.74
4.5 ± 0.5	1.07	2.73

ities (K_0 and G_0) were fitted as quadratic functions of the blood oxygen saturation using weighted least squares. These fits are shown in Fig. 3, and the corresponding parameter estimates and fit-quality assessments are listed in Table 2.

Combining the above results, the dependence of blood T_2 on the oxygen saturation, Y , and refocusing interval, τ_{180} , at 1.5 T, for the physiologically relevant hematocrit is best modeled by Eq. [2] with T_{20} of $203 \pm 3 \text{ ms}$, $r_c^2/2D$ of $4.60 \pm 0.42 \text{ ms}$, and G_0 given by:

$$G_0 = (4.50 \pm 0.51)10^{-13}[T^2] \left(1 - \frac{Y}{100}\right)^2. \quad [4]$$

T_1 Relaxometry

The Look-Locker data, obtained from the same set of blood samples (Hct = $51.2\% \pm 0.4\%$, mean \pm standard error), were fitted to a monoexponential recovery model via the nonlinear least-squares minimization. The dependence of the resulting T_1 estimates on Y was obtained by linear fitting of the spin-lattice relaxation rates. The results are shown in Fig. 4. The linear dependence of R_1 on Y is thus described as:

$$\frac{1}{T_1} = \frac{1}{996 \pm 36}[\text{ms}^{-1}] - (1.22 \pm 0.54)10^{-6} \left[\frac{\text{ms}^{-1}}{\%}\right] Y. \quad [5]$$

We investigated the effect of hematocrit on T_1 by using the above fit to compare the T_1 estimates based on the samples

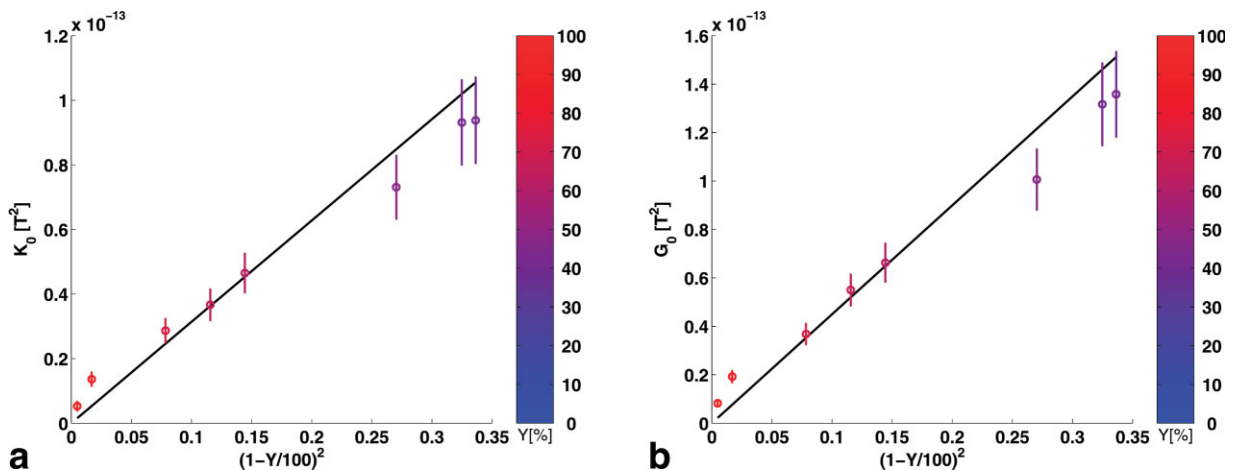


FIG. 3. K_0 estimates from the exchange model (a), and G_0 estimates from the diffusion model (b) fitted as quadratic functions of the oxygen saturation level.

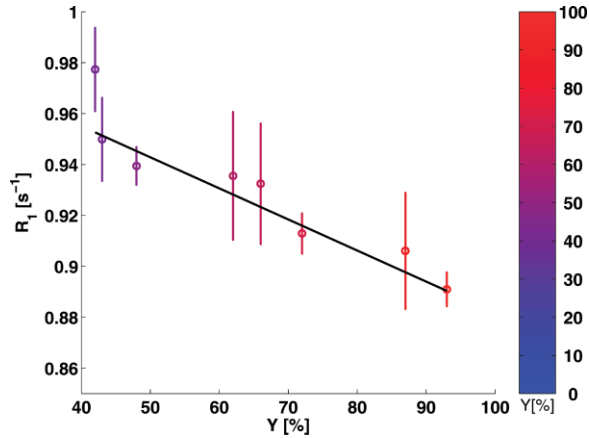


FIG. 4. The spin-lattice relaxation time of blood fitted against oxygen saturation for the blood samples employed with Hct of $51.2\% \pm 0.4\%$ (mean \pm standard error). The intercept estimate was $1/(996 \pm 36) \text{ ms}^{-1}$, and the slope, $dR_1/dY (-0.00122 \pm 0.00054) \times 10^{-3} \text{ ms}^{-1}\%$. The SSR was $1.05 \times 10^{-3} \text{ ms}^2$, and the NME was 4.22×10^{-3} .

with Hct of 51% to those obtained for a set of blood samples with Hct of 45%. A two-way ANOVA revealed a statistically significant effect ($F = 123$ and $P < 10^{-9}$) of hematocrit on the T_1 estimates when oxygen saturation was controlled for, with T_1 increasing with decreasing hematocrit.

DISCUSSION AND CONCLUSIONS

The current findings strongly support the use of the diffusion model over the fast chemical exchange model to describe the dependency of the spin-spin relaxation time in blood on oxygen saturation and refocusing interval at 1.5 T. In line with earlier studies (3,4,30), the dependence of the transverse relaxation rate shift on blood oxygen saturation was well modeled by a quadratic function. The model order optimization led to the selection of the constrained diffusion model, with a constant intrinsic transverse relaxation time. Even when T_{20} was allowed to vary with Y , we found no significant correlation of the resulting $T_{20,diffusion}$ estimates with oxygen saturation (data not shown). The slight variation in these estimates for different Y may have derived from small differences in the hematocrit of individual blood samples, in addition to noise.

In contrast, the quality of the exchange model fit significantly improved when the intrinsic transverse relaxation time was allowed to vary with oxygen saturation, with the $T_{20,exchange}$ estimates increasing linearly with Y , as reported previously (4). This preference for the Y -dependent $T_{20,exchange}$ may attest to the limitations of using the fast exchange formulation (being only just the “rapid” exchange limit achieved at 1.5 T (31)). While our exchange time estimate of $3.0 \pm 0.2 \text{ ms}$ lies well within the literature range of 0.6–10 ms (3–5,7,8,10,11,32), the limited applicability of the fast chemical exchange model to the present circumstances hinders the exact interpretation of this parameter (4,9).

The parameterizations obtained agree very well with those estimated by Jensen and Chandra (12) for the human whole-blood data published by Brooks et al (10). Specifically, for fully deoxygenated blood, the model of uniformly magnetized, randomly distributed spheres (i.e., Eq. [53] in Ref. 12), with $(4\pi\rho R^3/3)$ set to Hct) produced a G_0 estimate of $6.32 \times 10^{-13} \text{ T}^2$, compared to $(4.50 \pm 0.51) \times 10^{-13} \text{ T}^2$ predicted here (cf., Eq. [4]). The latter G_0 value corresponds to a susceptibility difference between plasma and fully deoxygenated erythrocytes of $(1.69 \pm 0.38) \times 10^{-7} \text{ cgs emu/cm}^3 \text{ Oe}$, or $(21.2 \pm 4.8) \times 10^{-3}$ in SI, the corresponding literature range being 1×10^{-7} to $3.5 \times 10^{-7} \text{ cgs emu/cm}^3 \text{ Oe}$ (2,16,17,31,33–35). In view of the limitations of the random spheres model (12), this agreement is reasonable. For Brooks et al.’s data with Y of 2% (10), Jensen and Chandra’s (12) fit produced a G_0 estimate of $4.16 \times 10^{-13} \text{ T}^2$ (scaled to 1.5 T), which is in excellent agreement with G_0 of $(4.32 \pm 0.49) \times 10^{-13} \text{ T}^2$ obtained from our Eq. [4]. The characteristic length scale for the spatial variations of the field inhomogeneities of $4.3 \pm 0.2 \mu\text{m}$ obtained is also in line with Jensen’s estimate of $4.2 \mu\text{m}$ (12). For the same data set, the present exchange model parameterization predicts a K_0 of $(3.01 \pm 0.15) \times 10^{-13} \text{ T}^2$, and an exchange time of $3.0 \pm 0.2 \text{ ms}$, compared to Jensen and Chandra’s (12) corresponding estimates of $2.60 \times 10^{-13} \text{ T}^2$ (again scaled to 1.5 T) and 3.6 ms, respectively.

It is important to stress that while our results support the use of Jensen and Chandra’s (12) diffusion model of spin-spin relaxation enhancement in partially deoxygenated blood over fast exchange at 1.5 T, they do not rule out some contribution of chemical exchange to R_2 enhancement. Furthermore, at fields above 1.5 T, a regime change (from rapid to intermediate exchange) occurs, so the chemical exchange contribution, in contrast to the diffusion one, does not scale with B_0^2 (31,34,36). As expected from the theoretical work of Brooks et al. (13), and clearly illustrated by the similarity of panels in Fig. 1, the chemical exchange model has the ability to reproduce the essential characteristics of the diffusion model. All that the present results demonstrate is that the diffusion model fits the data better. The quantification of the relative contributions of the two mechanisms is not achievable through the present comparison of the rather simplified descriptions of exchange and diffusion phenomena afforded by the models under investigation, and is beyond the scope of this study. Our primary objective here was to achieve a robust blood signal characterization in SE functional brain activation experiments using the best-performing model.

The parameterization of the diffusion model obtained allows ready evaluation of intravascular SE signal changes upon functional activation. Specifically, for a venous blood oxygen saturation change from 65% to 75%, and with the typical SE-BOLD TE of 100 ms, a venous blood transverse relaxation time elongation from 62 to 94 ms is predicted for a corresponding venous blood signal change of 74%. (However, the total intravascular SE-BOLD response will be determined by the relative volume contributions of the different vascular compartments and the changes in their respective oxygenation levels, which are dictated by activation-induced perfusion and oxygen consumption changes (2).)

With respect to spin-lattice relaxation, the observed increase of T_1 with decreasing Hct is in agreement with an earlier report (14). This phenomenon has been attributed to the higher protein content of red blood cells compared to plasma (37). Moreover, the rise in T_1 with the oxygenation level, which has been postulated to arise from direct (though limited) proton-dHb dipolar interactions (14), agrees with observations at 4.7 and 0.19–1.4 T (7,14) but not with a study at 1.5 T (15). A significantly smaller effect of Y on R_1 at 1.5 T compared to that reported at 4.7 T, in combination with limited sampling (only two oxygenation levels were probed in Ref. 15), may have precluded the detection of this dependency in the earlier 1.5 T study (15).

Two methodological notes regarding temperature and hematocrit should be made. Based on the published value of the *ex vivo* erythrocyte metabolism rate at 37°C (38), the expected drops in Y and pH over the course of the relaxometry measurements undertaken (~80 min) are $3\% \pm 1\%$, and 0.08 ± 0.03 pH units, and are thus within the standard error of the blood gas analyzer (as attested by the repeated measurements on the same blood samples that were performed to assess repeatability). A temperature of 22°C reduces the red blood cell metabolism even further, while the corresponding T_2 shortening is expected to be limited at 1.5 T over this range of temperatures (~5% decrease in T_2 from 37°C to 22°C (39)). On the other hand, the spin-lattice relaxation time is known to significantly decrease with decreasing temperature, by ~12% between 37°C and 22°C (40). In this study we did not investigate the dependence of T_2 on the hematocrit, since the application to normal brain physiology was the primary motivation for the experiment. The blood samples presently employed for spin-spin relaxometry were drawn from healthy, young adult males; however, the T_2 estimates derived from samples obtained from female volunteers, with Hct = 45–48%, showed the same functional dependence on Y and τ_{180} (data not shown). Over the physiological range of Hct (quoted as 30–50% (5)), a $\pm 15\%$ variation in T_2 has been reported (5). The mean squared magnitude of the field inhomogeneities, G_0 , in the diffusion model varies linearly with hematocrit (c.f., Eq. [53] of Ref. 12).

To ensure a robust prediction of blood relaxation rates, the experimental procedure included estimations of relaxation rates in samples with the same Hct and Y derived with different subjects, repeated refocusing interval measurements, and different acquisition strategies. Nevertheless, a comparison of the relaxation times thus estimated from literature values requires normalization for a series of experimental conditions, as is frequently emphasized. Notably, extrapolating the equations for R_2 (for long TE) given by Spees et al. (16) to our Hct values yields very good agreement. However, our T_2 values (c.f., Fig. 1c) are somewhat higher than those reported by Wright et al. (3). The venous T_2 range obtained here for very fast refocusing is also somewhat higher than that reported by Stadelmann et al. (39) ($T_2 \sim 146$ ms for venous blood at $\tau_{180} = 3$ ms). On the other hand, higher corresponding T_2 values were measured by both Golay et al. (4) and Silvennoinen et al. (14), which probably reflects the fact that their measurements were obtained at a higher temperature (37°) and lower hematocrit (44%).

In summary, the current findings provide support for the application of the recently reported model of diffusion in weak microscopic field inhomogeneities for describing the spin-spin relaxation rate enhancement in human whole blood at 1.5 T. The parameterization of this model in combination with the described linear decrease of spin-lattice relaxation rate with blood oxygen saturation allow the ready evaluation of intravascular blood signal changes for a given change in blood oxygen saturation at the selected refocusing interval. Moreover, an accurate quantification of physiological parameters of interest in methods that rely on dHb-induced T_2 shortening phenomenon is afforded.

ACKNOWLEDGMENTS

The authors thank Mr. Andre Cormier for constructing the wooden frame that allowed the blood samples to be securely fastened and well interfaced to the veristaltic pump. We also thank Prof. John G. Sled for helpful discussions and critical reading of this manuscript.

REFERENCES

- Sanders JA, Orrison WW. Functional magnetic resonance imaging. In: Orrison WW, Lewine JD, Sanders JA, Hartshorne MF, editors. Functional brain imaging. St. Louis, MO: Mosby Yearbook, Inc.; 1995. p 239–326.
- van Zijl PCM, Eleef SM, Ulatowski JA, Oja JME, Ulug AZM, Traystman RJ, Kauppinen RA. Quantitative assessment of blood flow, blood volume and blood oxygenation effects in functional magnetic resonance imaging. *Nat Med* 1998;4:159–167.
- Wright GA, Nishamura DG, Macovski A. Flow-independent magnetic resonance projection angiography. *Magn Reson Med* 1991;16:126–140.
- Golay X, Silvennoinen MJ, Zhou J, Clingman CS, Kauppinen RA, Pekar JJ, van Zijl PCM. Measurement of tissue oxygen extraction ratios from venous blood T_2 : increased precision and validation of principle. *Magn Reson Med* 2001;46:282–291.
- Thulborn KR, Waterton JC, Matthews PM, Radda GK. Oxygenation dependence of the transverse relaxation time of water protons in whole blood at high field. *Biochim Biophys Acta* 1982;714:265–270.
- Stefanovic B, Pike GB. Quantitative dynamic measurement of cerebral blood volume changes via fMRI. In: Proceedings of the 10th Annual Meeting of ISMRM, Honolulu, 2002. p 119.
- Gomori J, Grossman R, Yu-Ip C, Asakura T. NMR relaxation times of blood: dependence on field strength, oxidation state, and cell integrity. *J Comput Assist Tomogr* 1987;11:684–690.
- Bryant RG, Marill K, Blackmore C, Francis C. Magnetic relaxation in blood and blood clots. *Magn Reson Med* 1990;13:133–144.
- Gillis P, Peto S, Moyny F, Mispelter J, Cuenod CA. Proton transverse nuclear magnetic relaxation in oxidized blood: a numerical approach. *Magn Reson Med* 1995;33:93–100.
- Brooks RA, Vymazal J, Bulte JWM, Baumgarner CD, Tran V. Comparison of T_2 relaxation in blood, brain and ferritin. *J Magn Reson Imaging* 1995;4:446–450.
- Meyer BU, Roericht S, Graefin von Einsiedel H, Kruggel F, Weindl A. Inhibitory and excitatory interhemispheric transfers between motor cortical areas in normal humans and patients with abnormalities of the corpus callosum. *Brain* 1995;118:429–440.
- Jensen J, Chandra R. NMR relaxation in tissues with weak magnetic inhomogeneities. *Magn Reson Med* 2000;44:144–156.
- Brooks R, Moyny F, Gillis P. On T_2 shortening by weakly magnetized particles: the chemical exchange model. *Magn Reson Med* 2001;45:1014–1020.
- Silvennoinen M, Kettunen M, Kauppinen R. Effect of hematocrit and oxygen saturation level on blood spin-lattice relaxation. *Magn Reson Med* 2003;49:568–571.
- Barth M, Moser E. Proton NMR relaxation times of human blood samples at 1.5 T and implication for functional MRI. *Cell Mol Biol* 1997;43:783–791.

16. Spees W, Yablonskiy D, Oswood M, Ackerman J. Water proton MR properties of human blood at 1.5 T: magnetic susceptibility, T_1 , T_2 , T_2^* and non-Lorentzian signal behaviour. *Magn Reson Med* 2001;45:533–542.
17. Brooks RA, DiChiro G. Magnetic resonance imaging of stationary blood: a review. *Med Phys* 1987;14:903–913.
18. Conlon T, Outhred R. Water diffusion permeability of erythrocytes using an NMR technique. *Biochim Biophys Acta* 1972;288:354–361.
19. Gillis PS, Koenig H. Transverse relaxation of solvent protons induced by magnetized spheres: application to ferritin, erythrocytes, and magnetite. *Magn Reson Med* 1987;5:323–345.
20. Brindle KM, Brown FF, Campbell ID, Grathwohl C, Kuchel PW. Application of spin-echo nuclear magnetic resonance to whole-cell systems: membrane transport. *Biochem J* 1979;180:37–44.
21. Luz Z, Meiboom S. Nuclear magnetic resonance study of the protolysis of trimethylammonium ion in aqueous solution—order of the reaction with respect to the solvent. *J Chem Physics* 1963;39:366–370.
22. Matwiyoff N, Gasparovic C, Mazurchuk R, Matwiyoff G. The line shapes of the water proton resonances of red blood cells containing carbonyl hemoglobin, deoxyhemoglobin, and methemoglobin: implications for the interpretation of proton MRI at fields of 1.5 T and below. *Magn Reson Imaging* 1990;8:295–301.
23. Gasparovic C, Matwiyoff N. The magnetic properties and water dynamics of the red blood cell: a study by proton NMR lineshape analysis. *Magn Reson Med* 1992;26:274–299.
24. Brittain J, Hu B, Wright G, Meyer C, Macovski A, Nishamura D. Coronary angiography with magnetization-prepared T_2 contrast. *Magn Reson Med* 1995;33:689–696.
25. Levitt MH, Freeman R, Frenkiel T. Broadband decoupling in high-resolution nuclear magnetic resonance spectroscopy. *Adv Magn Reson* 1983;11:47–110.
26. Poon CS, Henkelman RM. Practical T_2 quantitation for clinical applications. *J Magn Reson Imaging* 1992;2:541–53.
27. Kay I, Henkelman R. Practical implementation and optimization of one-shot T_1 imaging. *Magn Reson Med* 1991;22:414–424.
28. Bland J, Altman D. Statistical methods for assessing agreement between two methods of clinical measurement. *Lancet* 1986;8476:307–310.
29. Packer K. The effects of diffusion through locally inhomogeneous magnetic fields on transverse nuclear spin relaxation in heterogeneous systems. Proton transverse relaxation in striated muscle tissue. *J Magn Reson* 1973;9:438–443.
30. Silvennoinen M, Clingman C, Golay X, Kauppinen R, van Zijl P. Comparison of the dependence of blood R_2 and R_2^* on oxygen saturation at 1.5 and 4.7 Tesla. *Magn Reson Med* 2003;49:47–60.
31. Matwiyoff N, Gasparovic C, Mazurchuk R, Matwiyoff G. On the origin of paramagnetic inhomogeneity effects in whole blood. *Magn Reson Med* 1991;20:144–150.
32. Herbst MD, Goldstein JH. A review of water diffusion measurement by NMR in red blood cells. *Am J Physiol* 1989;256:C1097–C1104.
33. Thulborn K, Waterton J, Matthews P, Radda G. Oxygenation dependence of the transverse relaxation time of water protons in the whole blood at high field. *Biochim Biophys Acta* 1982;714:265–270.
34. Wright GA. Magnetic resonance relaxation behaviour of blood: study and applications. Ph.D. thesis, Stanford University, Palo Alto, CA, 1991.
35. Weisskoff R, Kihne S. MRI susceptometry: image-based measurement of absolute susceptibility of MR contrast agents and human blood. *Magn Reson Med* 1992;24:375–383.
36. Lee T, Stainsby J, Hong J, Han E, Brittain J, Wright G. Blood relaxation properties at 3T—effects of blood oxygen saturation. In: Proceedings of the 11th Annual Meeting of ISMRM, Toronto, Canada, 2003. p 131.
37. Jiao X, Bryant R. Noninvasive measurement of protein concentration. *Magn Reson Med* 1996;35:159–161.
38. Greenbaum R, Nunn J, Prys-Roberts C, Kelman G. Metabolic changes in whole human blood (in vitro) at 37°C. *Resp Physiol* 1967;2:274–282.
39. Stadelmann H, Mueller E, Geibel K. Relaxationszeiten von venoensem Blut in Abhaengigkeit von der Feldstaerke. *Electromedica* 1991;59:82–88.
40. Lu H, Golay X, van Zijl P. What is the longitudinal relaxation time (T_1) of blood at 3.0T. In: Proceedings of the 11th Annual Meeting of ISMRM, Toronto, Canada, 2003. p 669.